International Journal of Thermal Sciences 49 (2010) 514–521

Contents lists available at ScienceDirect

International Journal of Thermal Sciences

journal homepage: www.elsevier.com/locate/ijts

Flow and heat transfer over shallow cavities

O.M. Mesalhy*, Salem S. Abdel Aziz, Mostafa M. El-Sayed

Mechanical Power Eng., Dept., Faculty of Eng., Zagazig University, Zagazig, Postal code 44519, Sharkia, Egypt

ARTICLE INFO

Article history:
Received 25 November 2008
Received in revised form
9 August 2009
Accepted 25 September 2009
Available online 6 October 2009

Keywords:
Shallow cavities
Heat transfer
Flow

ABSTRACT

The flow over a shallow cavity heated with constant heat flux form the bottom side has been studied experimentally and numerically. In the experimental part, pressure coefficient and Nusselt number have been measured along the cavity floor. In the numerical simulation, the conservation equations of mass, momentum, and energy have been solved. The standard k–ε turbulence model is used to account for the turbulent fluctuations. In both experimental and numerical part, the effect of changing cavity aspect ratio and Reynolds number has been studied. It is found that, a single elongated eddy has been formed for aspect ratio lower than 7. As the aspect ratio increases the flow impinges with the cavity floor creating two eddies, one beside the upstream cavity side and the second beside the downstream cavity side. Local Nusselt number along the cavity floor is affected mainly by the flow structure inside the cavity and the average Nusselt number has increased with increasing the aspect ratio up to 10 and with increasing Reynolds number. A correlation for the average Nusselt number, as a function of Reynolds number and cavity aspect ratio, is developed.

1. Introduction

The flow over cavities is of great interest as it is related to various engineering applications. These applications include solar energy collectors, combustion chambers, turbine blade tip flows, and flow through ribbed channels. Moreover, cavity flow represents a very important example of separated flow, which continuously receives more interest to understand its nature. In the literature many works dealing with this matter are found, but most of them are considering laminar flow over cavities and flow and heat transfer over cavities with small aspect ratios (deep cavities).

To show the flow structure of cavity flow, Sinha et al. [1], presented some experimental results for laminar flows over deep as well as shallow cavities. It was found that, the number and shape of the bubbles inside the cavity is influenced by its aspect ratio. Aung and Bhatti [2] studied numerically heat transfer for 2-D, laminar flow over cavities and they showed that heat transfer inside the cavity is strongly influenced by its aspect ratio. Experimentally, Aung [3] reported heat transfer data for laminar flows in cavities of aspect ratio varying from one to four. The results showed that, the local heat transfer distribution on the cavity floor has a maximum value located between the midpoint of the cavity floor and the downstream wall.

For turbulent flow regime over cavities, most of the previous researches concentrated on deep cavities, ribbed ducts, and grooved tips. Besides, some researchers introduced 2-D numerical simulations for shallow cavities. For deep cavities, Richards et al. [4] studied experimentally the turbulent heat transfer inside two-dimensional cavities with low aspect ratio. The Reynolds numbers that investigated, based on the cavity width, extended from 2×10^4 to 4×10^5. Four cavities with aspect ratios (height/width) of 1, 4/3, 2, and 4 were considered. The average heat transfer coefficients on the bottom of the cavities were measured and a correlation was obtained relating the Nusselt number based on the cavity height to the Reynolds number. It has been shown that the heat transfer rate was sensible to the aspect ratio of the cavity, and only marginally affected by the boundary layer thickness at the separation point.

Experimentally, Metzger et al. [5] studied heat transfer on a transverse grooved wall in a narrow flow channel, which is considered as a model for the flow through the clearance gap at the grooved tips of axial turbine blades. They concluded that the flow pattern is strongly dependent on the aspect ratio and little influenced by the variations in Reynolds number. Ooi et al. [6,7] numerically solved turbulent flow field and heat transfer in a 2-D grooved turbine blade and a 3-D ribbed duct. It was found that heat transfer predictions were not in good agreement with the experimental data for the 3-D ribbed duct. He attributed that to the presence of strong secondary flow structures which might not be properly simulated with turbulence models based on eddy viscosity. Matos et al. [8] conducted a 2-D Large Eddy Simulation for

* Corresponding author. Tel.: +20 010 728 7135.
E-mail address: Mesalhy_osa@yahoo.com (O.M. Mesalhy).

1290-0729/$ – see front matter © 2009 Elsevier Masson SAS. All rights reserved.
doi:10.1016/j.ijthermalsci.2009.09.007

Nomenclature

AR	cavity aspect ratio, L/H
C_p	pressure coefficient
c_p	specific heat at constant pressure, J/kg K
H	cavity height, m
K	turbulent kinetic energy, $(m/s)^2$
k	thermal conductivity of air, W/m K
L	cavity length, m
Nu_x	local Nusselt number
Nu_{aver}	average Nusselt number
p	static pressure, Pa
q''	heat flux, W/m^2
Re	Reynolds number
T	static temperature, K
U	mean velocity in the channel, m/s
u	velocity, m/s
W	channel width, m

Greek symbols

ρ	density, kg/m^3
ν	kinematic viscosity, m^2/s
ε	turbulence dissipation rate, m^2/s^3

Subscripts

inlet	cavity inlet
s	surface
∞	free stream
t	turbulent

turbulent flow over a plane symmetric cavity and over a free cavity. He concluded that the dynamic behavior of the cavity has a strong dependence on the geometry while it has a little dependence on Reynolds number.

Zdanski et al. [9–12] reported a series of numerical simulations of turbulent flow and heat transfer over 2-D shallow cavities. Regarding the flow structure, their predictions showed that the flow parameters were so sensitive to the variation of cavity aspect ratio, turbulence level of incoming flow, and Reynolds number. The flow results showed that, for some range of these parameters, the mean external flow does not touch the floor of the cavity. Their work had extended to study heat transfer for both laminar and turbulent flow regimes. A model based on Reynolds-averaged Navier–Stokes equations with the k–ε turbulence model was used. The results showed the influence of the flow structure on heat transfer and to the opposite behavior of the displacement of the two vortices inside the cavity for turbulent and laminar regimes inside the cavity.

Since, most of the researches in the literature review were dealing with laminar cavity flow, deep cavities, ribbed ducts, grooved tip flow, and 2-D numerical simulation of shallow cavities with isothermal bottom wall. This paper will present a parametric study of the flow field and heat transfer over shallow cavity heated from its bottom walls by a constant heat flux numerically and experimentally. A 3-D turbulent flow model will be adopted in the numerical simulation. Moreover, the range of the aspect ratio will be extended up to 17.4, which is not considered before. The influences of both aspect ratio and Reynolds number upon turbulent heat transfer inside the cavity will be studied.

2. Experimental set-up and measurements

The experimental work is conducted in an open wind tunnel with square cross section ($W = 44$ cm). Air is supplied to the test section, which has the dimensions of ($44 \times 44 \times 60$ cm) from a centrifugal fan pass through screen and honeycomb. Air gate at the fan inlet is used to change the mass flow rate of the air through the test section. Cavities of constant length, $L = 44$ cm, and with different heights, H from 2.52 to 7.86 cm, are attached in the lower wall of the test section. The layout of the test section with the cavity is shown in Fig. 1.

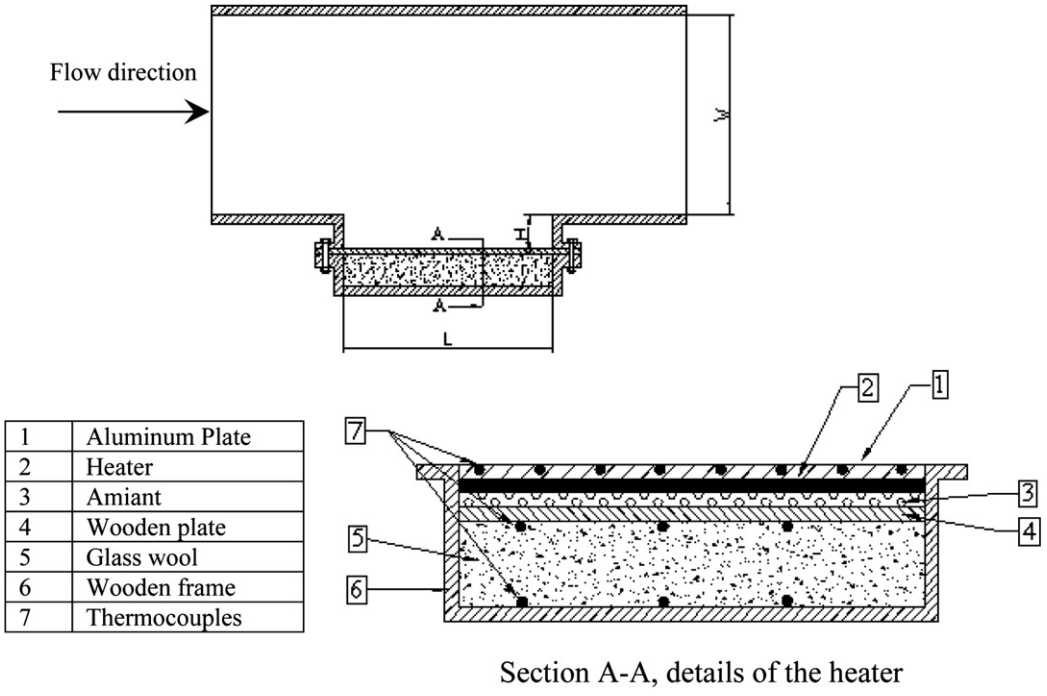

Fig. 1. Layout of the test section and the heater.

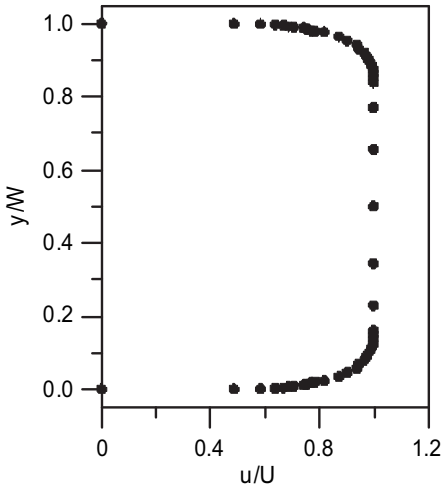

Fig. 2. Measured inlet velocity profile.

The bottom wall of the cavity is made of an aluminum plate (44 cm × 44 cm and 3 mm thick). The plate is heated electrically by a tape of Nickel chrome foil (4 mm width, and 0.2 mm thick). The Nickel chrome foil is wound over a mica sheet with spacing equal to 4 mm between any two neighboring foils. Then it is covered with another mica sheet. The electrical heater is fixed to the back of the aluminum plate, and is put in a wooden frame. The gap between the plate and the frame is insulated from all sides with 5 cm thick glass wool to minimize heat losses from the cavity, as shown in Section A–A in Fig. 1.

The heat input to the heater is controlled by an electric circuit composed of a 220 voltage regulator and power analyzer. The output of the voltage regulator is coupled to the heater through a wattmeter with accuracy of ±1% to generate a uniform surface heat flux.

For temperature measurements, forty-three Copper–Constantine thermocouples are installed in the surface of the Aluminum plate. The thermocouples are embedded equally spaced below the surface of the plate at a depth of 0.5 mm and the thermocouples are passed through equally spaced slots at the middle of the plate. In addition, to estimate the heat loss from the back face of the heater other surface thermocouples are fixed on the back face of the heater insulation and at 2.5 cm inside the glass wool insulation. The local Nusselt number is calculated based on cavity length, L, and the temperature difference $(T_s - T_\infty)$,

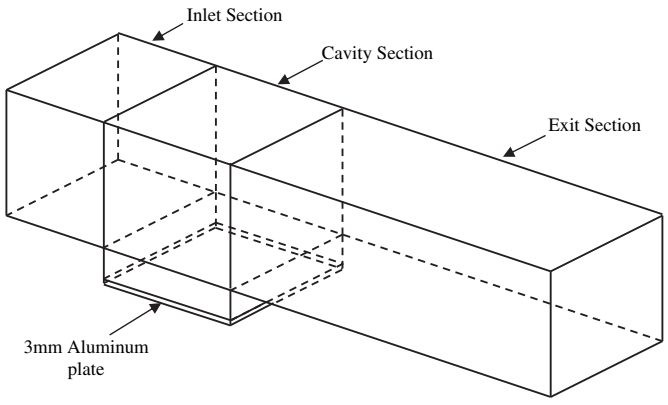

Fig. 3. Layout of the computational domain.

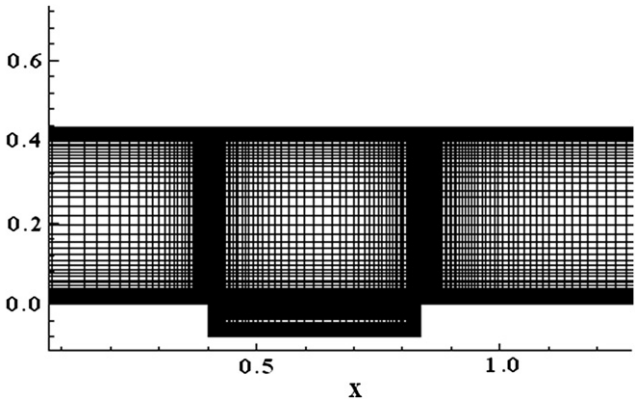

Fig. 4. Computational grid.

$$Nu_x = \frac{q''L}{k(T_s - T_\infty)} \tag{1}$$

The average Nusselt number is calculated from,

$$Nu_{aver} = \frac{1}{L}\int_0^L Nu_x dx \tag{2}$$

The calculated uncertainty in Nusselt number in our experiment was ±2.5% based on Kline and McClintok [13].

For pressure measurements, the bottom wall of the cavity is made of Plexiglas plate 6 mm thickness. Equally spaced static pressure taps are made at the middle of the Plexiglas plate to measure the static pressure distribution. The static pressure is measured by using micro-manometer referenced to the inlet free stream static pressure. The micro-manometer has an accuracy of ±2% at full-scale range of 10 mm H_2O. Then the pressure coefficient is calculated according to,

$$C_p = \frac{p - p_{inlet}}{\rho U^2/2} \tag{3}$$

The maximum uncertainty of pressure coefficient is calculated to be within ±1.3% based on Kline and McClintok [13].

The velocity profile at $x = 40$ cm upstream the cavity is measured using a pitot tube, which is taken as the inlet velocity profile in the numerical simulation. The inlet velocity profile is shown in Fig. 2. However, the turbulence intensity of the incoming flow is not measured and it is estimated to be 5% of the mean flow kinetic energy.

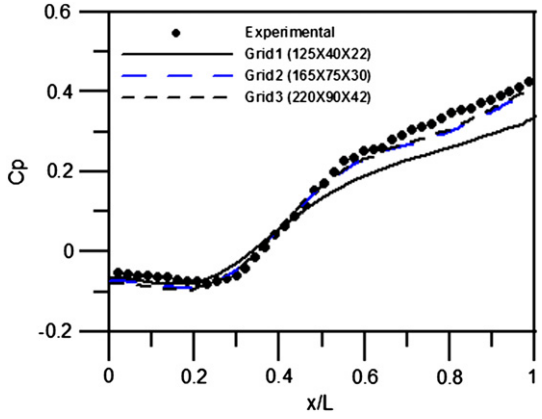

Fig. 5. Effect of changing the grid size (in the channel) on C_p, for aspect ratio = 9.6 and $Re = 2.2 \times 10^5$.

3. Numerical method

The numerical simulation is based on solving the Reynold's averaged Navier–Stokes equation on a 3-D geometry representing the test section that is adopted in the experimental work. The flow over the shallow cavity is considered to be steady, incompressible, and turbulent. The governing equations for such a flow are the time averaged of the conservation laws of mass, momentum, and energy, which can be written as follows,

Conservation of mass

$$\frac{\partial}{\partial x_i}(u_i) = 0 \tag{4}$$

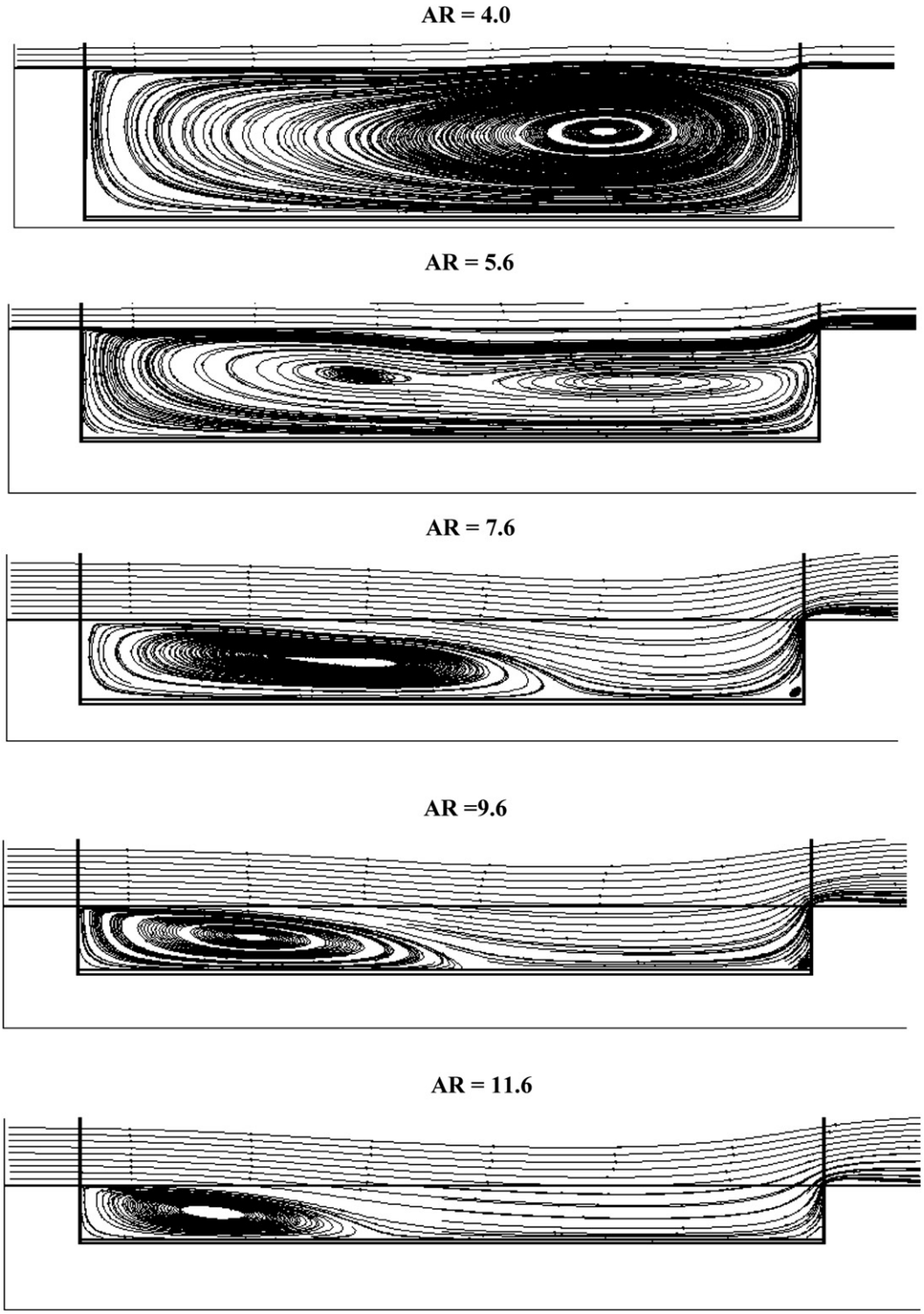

Fig. 6. Streamlines at the mid-section of the cavity for different AR at $Re = 2.2 \times 10^5$.

Conservation of momentum

$$\frac{\partial}{\partial x_i}(u_i u_j) = \frac{\partial}{\partial x_i}\left((\nu + \nu_t)\frac{\partial u_j}{\partial x_i}\right) - \frac{\partial p}{\rho \partial x_j} \quad (5)$$

Conservation of energy

$$\frac{\partial}{\partial x_i}(u_i T) = \frac{\partial}{\partial x_i}\left(\left(\frac{k}{\rho c_p} + \frac{\nu_t}{\sigma_t}\right)\frac{\partial T}{\partial x_i}\right) \quad (6)$$

where, ν_t and σ_t are the turbulent diffusivity and turbulent Prandtl number, respectively.

The standard k–ε model is selected to model the turbulent fluctuations of momentum and energy. The governing equations of K and ε can be written as,

$$\frac{\partial}{\partial x_i}(u_i K) = \frac{\partial}{\partial x_j}\left(\left(\nu + \frac{\nu_t}{\sigma_k}\right)\frac{\partial K}{\partial x_j}\right) + \frac{G_k}{\rho} - \varepsilon \quad (7)$$

$$\frac{\partial}{\partial x_i}(u_i \varepsilon) = \frac{\partial}{\partial x_j}\left(\left(\nu + \frac{\nu_t}{\sigma_\varepsilon}\right)\frac{\partial \varepsilon}{\partial x_j}\right) + C_{1\varepsilon}\frac{\varepsilon G_k}{\rho K} - C_{2\varepsilon}\frac{\varepsilon^2}{K} \quad (8)$$

where, G_k represents the generation of turbulent kinetic energy due to the mean velocity gradient, $G_k = \rho\overline{u_i' u_j'}(\partial u_j/\partial x_i)$, $C_{1\varepsilon}$ and $C_{2\varepsilon}$ are constants and σ_k and σ_ε are the turbulent Prandtl numbers for K and ε. The turbulent viscosity is calculated from, $\nu_t = C_\mu(k^2/\varepsilon)$, where C_μ is a constant of value 0.09. The standard wall function is used in conjunction with the k–ε model to bridge the viscosity-affected region beside the solid walls.

3.1. Calculation procedures

The numerical solution of the aforementioned governing equations has been carried out on a three-dimensional model representing the test section illustrated in Section 2 using the multipurpose commercial software FLUENT 6.3. FLUENT software is based on finite volume method on a collocated grid. The 3-D model is created and meshed using GAMBIT software, a geometric modeling and grid generation tool used with FLUENT. FLUENT is used to predict the pressure and temperature fields, which are compared with the experimental measurements.

3.2. Problem description and boundary conditions

Fig. 3 shows the computational domain. It consists of three sections; inlet, cavity, and exit sections. Due to symmetry, only half of the domain is considered. The dimensions of the domain are taken to fit exactly with the experimental set-up. The inlet section is extended upstream till the position at which we measured the inlet velocity profile. This measured profile is considered to be the inlet boundary condition in the numerical simulation. Also, turbulent intensity of a value 5% of the mean flow kinetic energy is specified at the inlet. In the experimental set-up, the bottom of the

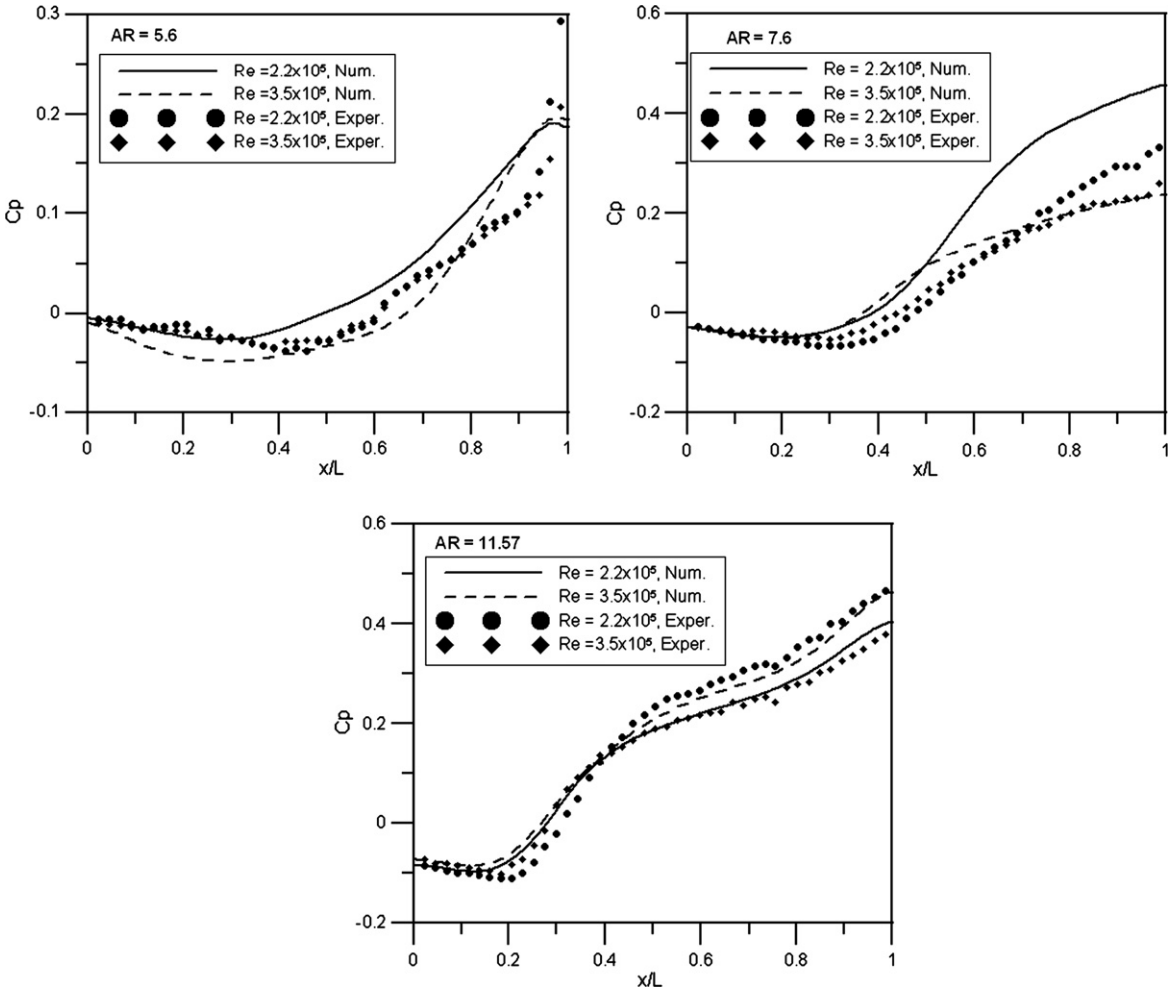

Fig. 7. Pressure coefficient along the cavity floor for different aspect ratios and Reynolds number.

cavity has manufactured from an Aluminum plate of thickness 3 mm. To account for the heat diffusion through that plate, it is considered in the computational domain and the heat flux from the heater is replaced by a constant heat flux at the bottom surface of the Aluminum plate. The boundary condition at the exit is considered to be a pressure outlet boundary, where we specified the pressure and all the other flow properties are extrapolated from the internal cells. The other surfaces of the model are considered to be adiabatic walls with no slip condition. The pressure–velocity coupling SIMPLE algorithm is used in the solution and a second order accurate finite difference scheme is used in discretization of the pressure correction equation while for momentum, energy, and turbulence equations, a second order upwind scheme is used.

An orthogonal mapped grid is generated for the channel blocks and for the cavity block. Fig. 4 shows the generated grid in a section parallel to x–y plane. A grid sensitivity study is carried out to find out the suitable grid size for that problem. As shown in Fig. 5, it is found that a grid of size ($165 \times 75 \times 30$ in x, y, and z directions, respectively) in the channel (plus the grid in the cavity block, which was varying with the aspect ratio) is suitable. The grid is concentrated besides the walls and besides the cavity corners, where high velocity and temperature gradients are expected.

4. Results and discussions

In this section we present the results of turbulent flow over a heated shallow cavity. The main parameters that we have changed are the cavity aspect ratio, AR, and Reynolds number, Re. The aspect ratio has changed from 4 to 17.4. The mean air velocity in the channel has changed from 5 m/s to 18 m/s, which give Reynolds number calculated based on the cavity length, in the range ($Re = 1.4 \times 10^5$–4.92×10^5). Our main objective is to find out the effect of changing Re, and cavity aspect ratio on convective heat transfer from the cavity bottom.

4.1. Flow results

It is noticed from the numerical results that the flow inside the cavity is affected mainly by the cavity aspect ratio. Fig. 6 shows the predicted streamlines at the mid plane of the cavity for different aspect ratios. As shown from the figure, for small aspect ratio, AR = 4, and 5.6, the cavity behaves like a shallow open cavity. The flow in this type is characterized by a single elongated eddy. Inside the bigger eddy, two smaller eddies are formed, one near to the left side and the other near to the right side of the cavity. As the aspect ratio increases, the cavity flow behaves like shallow closed cavity. In our numerical study we have noticed that this occurs for aspect ratio greater than 7. This kind of flow is characterized by generating a bubble behind the upstream face of the cavity. Another bubble may generate in front of the downstream face of the cavity. Also the flow in this type has the chance to impinge with the cavity floor. The location at which the flow impinges with the cavity floor changes with changing the aspect ratio and with the mean channel air velocity.

To verify the numerical results with the experimental data, the measured pressure coefficient, C_p, along the mid plane of the cavity floor is compared with the numerical results. Fig. 7 shows this comparison for three different aspect ratios, AR = 5.6, 7.6, and 11.57. As shown in the figure, there is a region for which the pressure coefficient is negative; this corresponds to the recirculation bubble formed behind the left side wall of the cavity. The region of high pressure starts at the impinging point (or the point of reattachment) of the flow with the cavity floor. The static pressure increases as we move to the right side wall of the cavity. For low aspect ratio, the negative pressure region occupies most of the cavity space. This happens for aspect ratios lower than 6. As the aspect ratio increases the C_p is getting more negative and the region of negative pressure displaces to the left. The numerical and the experimental results follow the same trend as shown in the figure. However, we have

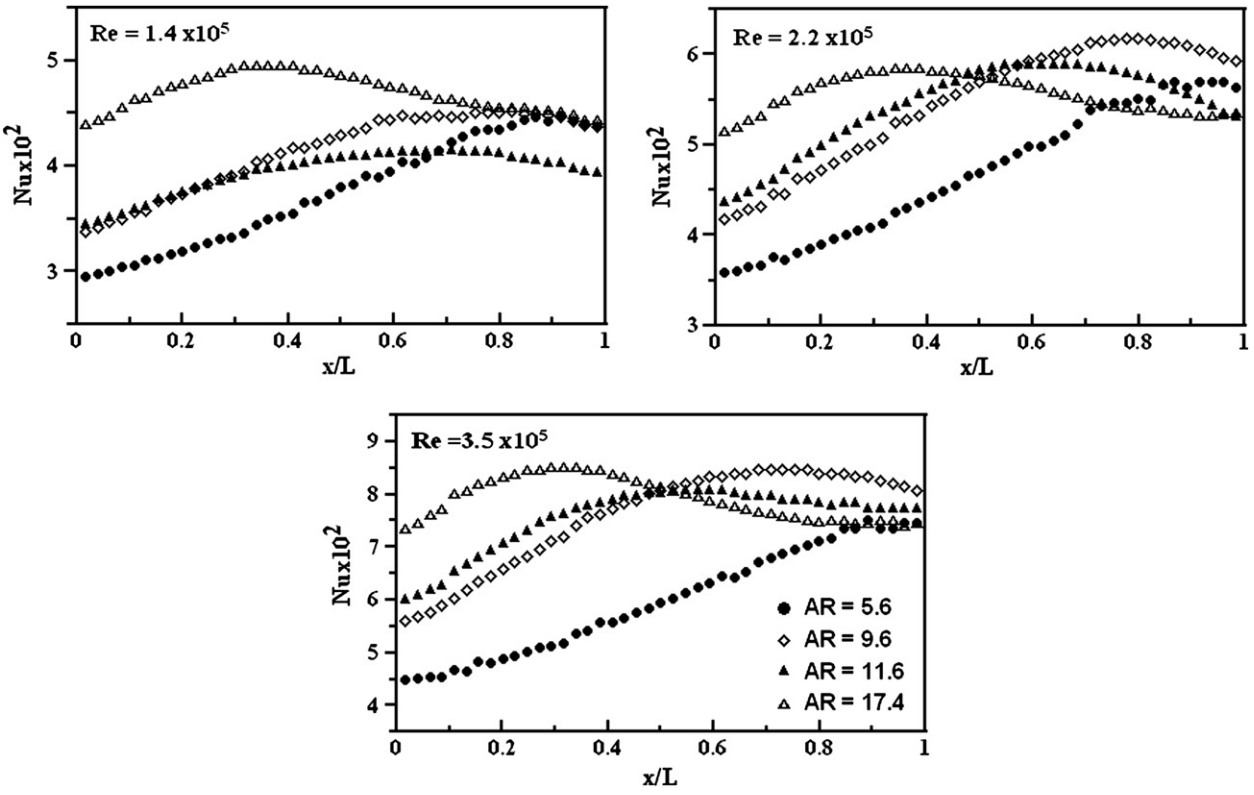

Fig. 8. Local Nusselt number along the cavity floor for different aspect ratios and different Reynolds number.

seen a difference between the predicted and the measured location of the point of minimum pressure, which corresponds to the center of the generated bubble beside the upstream cavity wall.

4.2. Heat transfer results

Heat transfer results have been shown in terms of local and average Nusselt numbers, Nu_x, and Nu_{aver}, respectively. Flow structure inside the cavity is expected to have the great impact on heat transfer results. The locations, where vortices are formed, are expected to have low heat transfer coefficients while the Nusselt number is expected to reach its maximum value beside the impinging point.

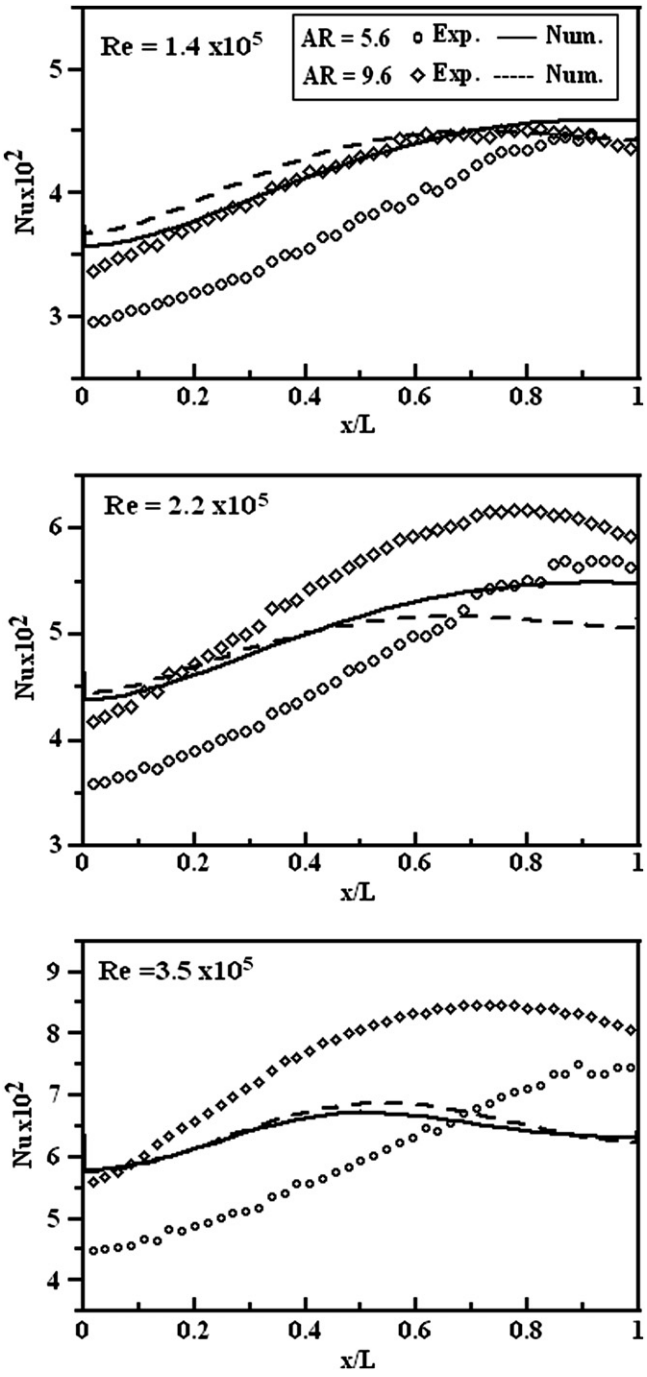

Fig. 9. Comparison between experimental and numerical local Nusselt number.

4.2.1. Effect of aspect ratio

Fig. 8 shows the measured local Nusselt number for different values of aspect ratio. The figure shows the distribution of the local Nusselt number along the cavity floor. As can be seen, the local heat transfer coefficient has low value beside the upstream side of the cavity (the region where the large bubble is formed). For aspect ratio 5.6 it is found that the distribution of Nusselt number does not show a maximum point. The value of Nusselt number is lower beside the cavity upstream side and increases as we move to the right side of the cavity. This is due to the formation of a single bubble, which induces the fluid at the shear layer to rotate inside the cavity. During the fluid circulation it touches the cavity floor first at the downstream side and moves in the opposite direction of the flow to the upstream side. As the aspect ratio increases, the local Nusselt number shows a maximum point. We considered that the point at which the local Nusselt number, Nu_x, reaches its maximum value is the point of the flow impingement with the cavity floor or the point of reattachment. The location of this point displaces to the left as the aspect ratio and the free stream velocity increases, as shown in the figure.

The numerical results for the local Nusselt number showed the same trend, but we have noticed some discrepancies between the model and the measurements. The numerical model (k–ε with wall function) fails somehow to predict the exact values of Nu_x and the point of reattachment or impingement (the point at which maximum Nu_x occurs) especially at higher values of Reynold's number. This can be attributed to the complex nature of this 3-D cavity flow where separation, reattachment, and secondary flow exist. A more accurate turbulence model may be needed (Reynolds stress model or Large Eddy Simulation). Also, neglecting the effect of natural convection in the numerical model may be responsible to this deviation. The comparison between the experimental and numerical results is shown in Fig. 9.

The average Nusselt number is calculated along the cavity floor and it is compared with the nearest case in the literature, which was the case of one-sided ribbed duct of aspect ratio equal to 6, 8, 9, 10, and 12 [14]. Although the two cases are quite different, the results showed the same trend as shown in Fig. 10 but the ribbed channel was associated with higher average Nusselt number.

The average Nusselt number of the current experimental work is plotted at different Reynold's number as shown in Fig. 11. It is noticed that the average Nusselt number increases as the aspect ratio increases from 5 to 10. This range of aspect ratio includes the aspect ratio at which the cavity flow changes from behaving like an open cavity to a closed cavity. It is found that increasing aspect ratio

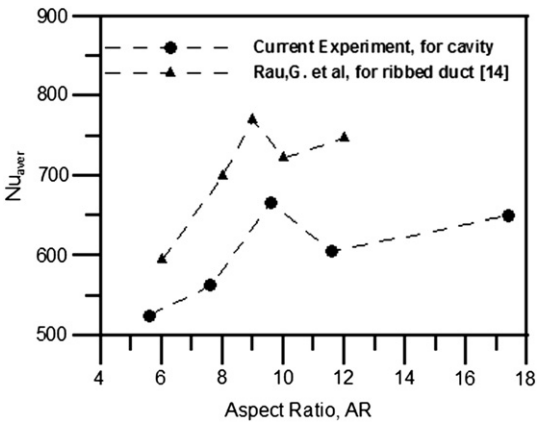

Fig. 10. Comparison between the current experiment and experimental data for ribbed duct, $Re = 2.2 \times 10^5$.

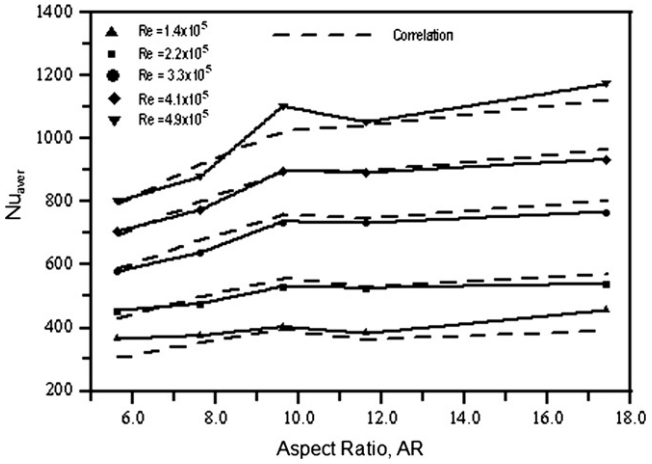

Fig. 11. Effect of changing cavity aspect ratio on average Nusselt number.

more than 10 does not make a big change in the average Nusselt number.

4.2.2. Effect of Reynold's number

As can be seen from Fig. 11, the average Nusselt number increases uniformly with *Re*. But we can observe from the figure that the lines of constant *Re* diverge as we move towards higher aspect ratios. This can be interpreted by distinguishing between the flow-type corresponding to the aspect ratio. For lower aspect ratios the heat transfer is affected mainly by vortices created inside the cavity. But for higher aspect ratio, the heat transfer is affected mainly by the impingement of the mean flow with the cavity floor.

A correlation has been developed for the average Nusselt number as a function of Reynolds number and cavity aspect ratio. Due to the nature of cavity flow, it was found that it is useful to make this correlation for two ranges of aspect ratio, one for aspect ratio less than 10 and the other for aspect ratio greater than 10. This correlation takes the following form,

$$Nu_{\text{aver}} = 0.0164\, Re^{0.76}\, \text{AR}^{0.474} \text{ for AR} < 10$$

$$Nu_{\text{aver}} = 0.0107\, Re^{0.84}\, \text{AR}^{0.182} \text{ for AR} > 10$$

The average error in this correlation was found to be less than 4.5%. This correlation is valid only for air ($Pr = 0.71$) and for the data range that has been used to develop it ($1.4 \times 10^5 < Re < 5 \times 10^5$, and $5 < \text{AR} < 18$).

5. Conclusions

Shallow cavities are used in many applications especially as a wind barrier in solar collectors. Shallow cavities can make a compromise between reducing the convection losses and shadowing effect in the solar collector. In this study, the flow over shallow cavities heated with constant heat flux from the bottom side has been studied experimentally and numerically. The effect of changing cavity aspect ratio and Reynolds number on flow field and heat transfer has been studied. The aspect ratio of the cavity is extended up to 17.4. The numerical and experimental results showed the same trend but there were some discrepancies between numerical and experimental results in predicting the reattachment point and local Nusselt number. It can be concluded that based on the value of the cavity aspect ratio, the type of cavity flow changes from open cavity flow to closed cavity flow. The critical aspect ratio at which this change occurs was around 7. The cavity flow-type was the key parameter that figured out the heat transfer process since the vortices formed inside the cavity could make an insulation effect to the heat transfer from the cavity floor. It was found that, the average Nusselt number (heat losses) increased as the aspect ratio increased up to 10 but no considerable changes occurred as the aspect ratio increased more than this value. The effect of changing *Re* on the heat transfer process sounded more for higher aspect ratio cavities because the heat transfer was affected mainly by the impingement of the mean flow with the cavity floor. A correlation has been developed for the average Nusselt number as a function of Reynold's number and cavity aspect ratio.

References

[1] S.N. Sinha, A.K. Gupta, M.M. Oberai, Laminar separating flow over backsteps and cavities, part II: cavities. AIAA Journal 20 (3) (1982) 370–375.
[2] W. Aung, A. Bhatti, Finite difference analysis of laminar separated forced convection in cavities. Journal of Heat Transfer 106 (1) (1984) 49–54.
[3] W. Aung, An interferometric investigation of separated forced convection in laminar flow past cavities. Journal of Heat Transfer 105 (3) (1983) 505–512.
[4] R.F. Richards, M.F. Young, J.C. Haiad, turbulent forced convection heat transfer from a bottom heated open surface cavity. International Journal of Heat Mass Transfer 30 (1987) 2281–2287.
[5] D.E. Metzger, R.S. Bunker, M.K. Chyu, Cavity heat transfer on a transverse grooved wall in a narrow flow channel. Journal of Heat Transfer 111 (1) (1989) 73–79.
[6] A. Ooi, G. Iaccarino, M. Behnia, Heat Transfer Predictions in Cavities, Annual Research Briefs. Center for Turbulence Research, NASA Ames/Stanford Univ., 1998, pp. 185–196.
[7] A. Ooi, G. Iaccarino, P.A. Durbin, M. Behnia, Reynolds averaged simulation of flow and heat transfer in ribbed ducts. International Journal of Heat and Fluid Flow 23 (2002) 750–757.
[8] A. Matos, F.A.A. Pinho, A.S. SilveriraNeto, Large-eddy simulation of turbulent flow over a two-dimensional cavity with temperature fluctuations. International Journal of Heat Mass Transfer 42 (1999) 49–59.
[9] P.S.D. Zdanski, M.A. Ortega, G.C.R. Nide, Fico, Jr., Numerical simulations of turbulent flows over shallow cavities, in: Proceedings of the 2nd Int. Conference on Computational Heat and Mass Transfer, 2001, Oct. 22–26
[10] P.S.B. Zdanski, M.A. Ortega, G.C.R. Nide, Fico Jr., Numerical study of the flow over shallow cavities. Computer and Fluids 32 (2003) 953–974.
[11] P.S.B. Zdanski, M.A. Ortega, G.C.R. Nide, Fico Jr., Heat transfer studies in the flow over shallow cavities. Journal of Heat Transfer, ASME 127 (2005) 699–712.
[12] P.S.B. Zdanski, M.A. Ortega, G.C.R. Nide, Fico Jr., On the flow over cavities of large aspect ratio: a physical analysis. International Communications in Heat and Mass Transfer 33 (2006) 458–466.
[13] J. Kline, F.A. McClintok, Describing uncertainties in single-sample experiments. Mechanical Engineering 75 (1953) 3–8.
[14] G. Rau, M. Cakan, D. Moeller, T. Arts, The effect of periodic ribs on the local aerodynamic and heat transfer performance of a straight cooling channel. Journal of Turbomachinery 120 (1998) 368–375.